

**Integrate-and-fire model of disease transmission**

Shahbanno A. Hussain , David C. A. Meine , and Dimitri D. Vvedensky   
*The Blackett Laboratory, Imperial College London, London SW7 2AZ, United Kingdom*

 (Received 27 March 2024; accepted 4 July 2024; published 24 July 2024)

We create an epidemiological susceptible-infected-susceptible model of disease transmission using integrate-and-fire nodes on a network, allowing memory of previous interactions and infections. Agents in the network sum infectious matter from their nearest neighbors at every time step, until they exceed their infection threshold, at which point they “fire” and become infected for as long as the recovery time. The model has memory of previous interactions by tracking the amount of infectious matter carried by agents as well as just binary infected or susceptible states, and the model has memory of previous infections by modeling immunity as increasing the infection threshold after recovery. Creating a simulation of the model on networks with a power-law degree distribution and homogeneous agent parameters, we find a single strain version of the model matches well with the England COVID-19 case data, with a root-mean-squared error of 0.014%. A simulation of a multistrain version of the model (where there is cross-strain immunity) matches well with the influenza strain A and strain B case numbers in Canada, with a root-mean-squared error of 0.002% and 0.0012%, respectively, though due to the coupling in the model, both strains peak in phase. Since the dynamics of the model successfully capture real-life transmission dynamics, we test interventions to study their effect on case numbers, with both quarantining and social gathering restrictions lowering the peak. Since the model has memory, the stricter the intervention, the higher the secondary peak when the restriction is removed, showing that interventions change only the shape of the curves and not the overall number infected in the population.

DOI: [10.1103/PhysRevE.110.014305](https://doi.org/10.1103/PhysRevE.110.014305)

**I. INTRODUCTION**

The importance of epidemiological modeling has been rekindled following the SARS-CoV-2 (COVID-19) pandemic. Accurate models of epidemiological transmission are powerful forecasting tools that mimic how diseases are transmitted across populations and help to inform governmental policies [1]. A simple epidemiological model is the susceptible-infected-recovered (SIR) model, where the infection transmission rate between susceptible and infected individuals (agents), and the rate at which they recover, is constant and uniform across the population. For a large population, we can assume meetings between agents are random and equally likely, i.e., the population is “fully mixed,” which allows differential equations to be solved for the number of infected individuals over time [2]. However, these models do not account for social structure. For example, agents are more likely to come into contact with certain groups, such as family members.

The social structure of a population can be modeled by a network [3]. A network is a collection of nodes that are connected to each other by edges. The nearest neighbors of a node are the set of nodes that are connected to that node

by exactly one edge. The number of edges a node has (i.e., the number of nearest neighbors) is called the degree of the node. Utilized in epidemiological models, nodes represent individuals, edges represent social connections, and the edges become “occupied” if infection has been transmitted between the two agents [4]. Weights can be assigned to the nodes in spiking networks, such that if the threshold is exceeded, secondary transmission can occur between individuals [5], though this fails to integrate over multiple interactions over time, i.e., there is no memory of previous interactions.

There are several variations of the SIR model. Modifications include additional states [6,7], complex networks [8–10], and the effects of memory [11–16]. In the SIR-resusceptible (SIRS) model, recovered agents lose immunity at a given rate to return to being susceptible [6]. Once an agent is immune to one strain of a virus, the transmission rate for contracting other strains is given by the corresponding entry in a cross-immunity matrix [7]. Due to the biological competition exclusion principle, more infectious strains will overcome weaker strains with time [17]. However, these models do not have memory of previous infections—a susceptible individual who has never been infected is treated identically to a susceptible individual who has been infected multiple times. Studies of complex networks have included the effect of network topology, such as degree and connectedness, on the spread and extinction of a virus [9], and the movement of random walkers on complex networks as a measure of effective distance, linking diffusion with disease spreading [8], and with independent random walkers modeling survival and mortality [10].

---

*Published by the American Physical Society under the terms of the Creative Commons Attribution 4.0 International license. Further distribution of this work must maintain attribution to the author(s) and the published article’s title, journal citation, and DOI.*

Memory is essential for modeling the spread of a disease, especially over short timescales [18] and through exposure history, perhaps involving multiple diseases, over all timescales [19]. In the SIR model, memory effects can be included in the dynamics of the individual susceptible, infected, and recovered populations by convolution integrals [11]. There are several other ways in which memory has been included in epidemiological models, including the network on which agents reside [12], past exposures to multiple sources of infection [13], random immunity time after recovery [14], and distributions of exposure and recovery times [15,16]. The various approaches to the modeling of the spread of diseases have been reviewed from several points of view [19–22].

The integrate-and-fire model is a neurological transmission model first developed to capture the traversal of electrical signals across neurons [23]. Incoming currents from neighboring neurons are summed until the threshold is reached, at which point the neuron fires and the signal is transmitted. The neuron then becomes inactive, i.e., stops receiving signals, for the length of time known as the refractory time, before becoming active again. The activity of a population of neurons can be defined by the number of spiking neurons over a time interval divided by the time interval and the total number of neurons [24].

Integrate-and-fire neurons have been used to model the spread of social contagions on a scale-free online social network [25], where the summation of current represents receiving information from different sources, the firing threshold represents the point where agents publish a message online, and the refractory period where the agent is insensitive to new information and is inactive. The parameters in the simulated network were tuned to match empirical results from Twitter for varying, internal and external input current sources [25], highlighting the potential future predictive power of such a model.

Here, we create a model of disease transmission which uses (i) a network to model social structure, (ii) integrate-and-fire nodes to sum infectious matter from neighbors to give memory of previous interactions, and (iii) changing of the infection threshold on recovery, so susceptible agents are no longer identical and have memory of previous infections. This better capture features observed in real-life case numbers, such as secondary waves of infection. A more representative model can be used to reliably test different interventions, such as different levels of quarantines and gathering restrictions, helping better inform policies and responses to epidemics.

The outline of our paper is as follows. We formulate our model and investigate its parametrization using simulations in Sec. II. The effectiveness of a single-strain version of the model in capturing real-life dynamics is evaluated in Sec. III. The model has memory of previous interactions by tracking the amount of infectious matter carried by agents, and memory of previous infections by modeling immunity as increasing the infection threshold after recovery. Various types of intervention are simulated in Sec. IV to evaluate their effectiveness in reducing the spread of infection. Section V extends the model to account for multiple strains. The main conclusions of this paper are summarized in Sec. VI, which includes directions for further work. The Supplemental Material (SM) [26] contains the mathematical formulation of

TABLE I. Identification between the elements of a neurological integrate-and-fire model and the agents in our epidemiological model.

Integrate-and-fire	Epidemiology
Voltage	Amount of infectious matter
Spiking threshold	Infection threshold
Refractory time	Recovery time

our model, the parameters that are used, the effect of varying the parameters, and the corresponding plots.

## II. THE MODEL

Social structure is an important factor governing how infections that transmit through close-contact interactions spread through a society. Therefore, we use a network where nodes are agents and unweighted edges between them are connections. Nodes follow a power-law degree distribution with an exponent of 3, which replicates social networks observed in nature [27]. Its scale-free nature [28] means that simulations can be run on smaller system sizes, while retaining the social structure observed in much larger populations. We consider a fixed population size (i.e., no births or deaths) and, thus, a fixed number of nodes within the network.

We use integrate-and-fire nodes, where we sum the amount of infectious matter between agents instead of current [23]. The spiking threshold becomes the infection threshold, i.e., the amount of infectious matter required in the body of an agent to be declared infected, and the refractory time (where the neuron is inactive and stops receiving further inputs) corresponds to the recovery time. These identifications are summarized in Table I. Agents can be either susceptible or infected.

### A. Integrate

Each agent begins with a given amount of infectious matter: either zero or nonzero from random initial injection. At every time step, all agents transmit their amount of infectious matter to their nearest neighbors (without depleting their own amount), dividing it equally among all their connections to avoid bias on any neighbor. Transmissions are scaled inversely proportional to the degree, as it is unreasonable for high degree agents to transfer equally to all their connections, so this indirectly takes into account spatial distances. The outgoing infections from infected and susceptible agents also have transmission probabilities, which is the fraction of infectious matter that is transmitted, to take into account that not all matter is transmitted.

The receiving agents, if in the susceptible state, add the incoming infection to their current infection amount, such that meeting someone carrying a higher amount of infectious matter increases the amount in their body proportionally. This gives agents memory of previous interactions. Infected agents no longer sum infectious matter from their neighbors, but still transmit, as they are now actively ill and no longer need to contract more infectious matter. The amount of infectious matter carried by infected and susceptible agents decays exponentially with the respective characteristic time constants to represent the body naturally fighting against the disease.

TABLE II. The model parameters, their interpretation, and their effects on new cases over time deduced from simulations in the SM [26].

Parameter	Interpretation	Effect on new cases over time
Number of agents	Number of nodes, population	All collapse onto same shape in plot of new cases as percentage of total population. Power-law network is scale free [28], so same transmission dynamics leads to same results.
Spiking threshold	Infection threshold	Effect of changing the threshold is the same as infecting 100% of the population with a given infectious matter amount.
Refractory time	Recovery time	Increasing refractory time increases the time between peaks.
Transmission rate	Fraction of infectious matter transmitted from agent at each time step	Decreasing transmission rate of susceptible agents delays time to first peak. Decreasing transmission rate of infected agents increases time between peaks and decreases heights of all peaks.
Threshold factor	Immunity upon recovery	Increasing this factor reduces the number of peaks, increases time between peaks, and lowers heights of subsequent peaks.
Immunity decay constant	Natural loss of immunity over time	Decreasing the time constant (i.e., stronger loss of immunity) makes subsequent peaks occur sooner.
Infectious matter decay constant	Body fighting against infection	Decreasing the time constant delays time to first peak and decreases the heights of peaks.
Initial percentage of agents with infectious matter	Fraction of population with initially nonzero infectious matter	Increasing the percentage initially infected shifts peaks in cases to earlier times.
Percentage of threshold initially injected into given agents	How close agents who are injected with infectious matter are to infection	Increasing the amount by which agents are infected shifts peaks earlier and lowers heights of all peaks. The more total infection in the system, the more substantially the peaks shift.

**B. Fire**

An agent becomes infected when the amount of infectious matter exceeds their infection threshold, analogous to a neuron “firing.” The time at which this happens is registered as a new case. Agents remain in the infected state for as long as the recovery time. Once recovered, the agent’s infection amount is reset to zero to symbolize successfully having fought off the virus, at which point they return to the susceptible state (and begin acquiring infectious matter again). However, we assume the agent now has some immunity to the infection, so we increase their infection threshold by a fixed factor, called the immunity threshold factor, to represent how more infection will be needed for them to become infected again. This gives agents in the model memory of previous infections.

This may mean that there is an unnaturally higher average amount of infectious matter in the system, as previously infected agents can withstand a much larger infection amount and thus transmit their larger amount to their neighbors which have lower thresholds. To counteract this, outgoing transmission is also scaled by an output factor, which is equal to the reciprocal of the product of all of the threshold factor increases so far for the given agent, i.e., the inverse to the changes in threshold. To represent the loss of immunity over time, the infection threshold exponentially decays with a characteristic time constant, though not lower than the initial base value.

**C. Parameters**

We simulate the model in PYTHON [29] to test and uncover the features described here. We consider perturbations of each parameter in a simple version of the model to discern their effect on case numbers, summarized in Table II, with explanations uncovering features of the dynamics of the model. The

base parameters that are used and the corresponding graphs are listed in the SM [26]. Agent parameters are homogeneous, with agents differing only by their degree and amount of initial infectious matter.

**D. Features of  $N = 2$  observed for  $N > 2$**

Figure 1(a) shows the maximum number of new cases following the base parameters in Table I of the SM [26], against the infectious matter decay constant (Table II) with

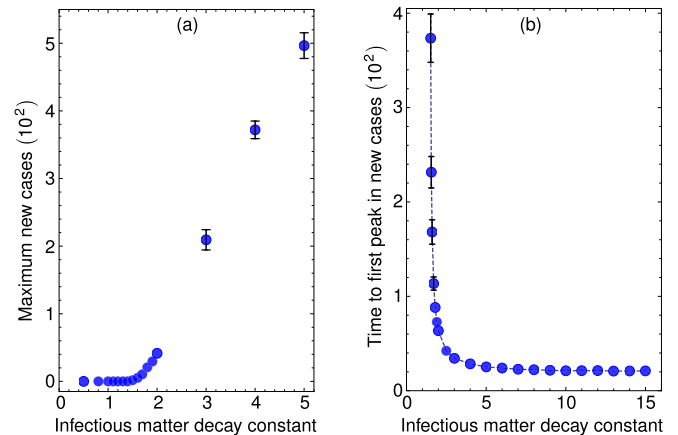


FIG. 1. (a) Average maximum number of new cases and (b) average time to first peak in new cases, both against the infectious matter decay constant. Blue points indicate simulations in (a) and (b) using parameters in Table I of the SM [26], with the error obtained by the standard deviation from 100 runs. Where no error bar is indicated, the circle is larger than the error. In (a), when the time constant is less than  $1/\ln 2$ , there are no new cases. In (b), the blue dotted line is obtained from theory from (5) of the SM [26], with  $\bar{I}(0)$  adjusted for 2500 agents (as in the simulation).

parameter  $\tau$ . We notice that despite the simulation having 2500 agents and immunity, it remarkably matches the analytical result obtained for the two-agent case in Sec. IA in the SM [26], where a clear cutoff is observed in the number of cases for  $\tau < 1/\ln 2$  (for initial conditions where no agent is at the threshold). Since outgoing transmissions are scaled by degree, the maximum possible transmission occurs in a two-agent system, where all agents in the system have a minimum number of connections (degree 1). Therefore, it follows that if  $\tau < 1/\ln 2$  suppresses infection in the maximum transmission case, it also suppresses transmission for larger populations. Note that this is the only condition in the model that leads to no epidemic. Otherwise, given enough time, the infection will eventually spread through the network.

Figure 1(b) shows the time to first peak in new cases against the infectious matter decay constant, for simulation results obtained for 2500 agents, and the analytical result for two agents from (5) of the SM [26] [adjusting the quantity  $\bar{I}(0)$  for 2500 agents]. It is remarkable that the result derived for the time to first infection in the system for two agents is consistent with the time to *first peak* in new cases for larger system sizes. This means the time to peak infection is independent of system size, consistent with the network being scale free [28], and with the results in Table II, where only the infectious matter decay constant and initial conditions change the time to the first peak. This also means that we can use the analytical result in (5) from the SM [26] to calculate the time to peak new cases for any system size, without having to use a simulation.

### III. SINGLE STRAIN

#### A. Real-life data set

We study the spread of COVID-19 due to close-contact human interactions, i.e., the main mode of transmission [30]. We use case data from England [31], where we take weekly averages of the number of received positive test specimens to account for fluctuations in individuals taking tests, thereby alleviating the drop towards the end of the week. We consider data from February 24, 2022 onwards, when legal restrictions officially ended [32], to see if the model can replicate the natural spread of infection without human intervention. During this period, only the Omicron variant of COVID-19 predominantly remained [31], allowing us to use a single-strain version of the model.

#### B. Tuning the model

Since the exact distribution of infection throughout the population is unknown at the time of ending restrictions, we let the infection organically spread in the simulation by injecting only a small amount of infectious matter into the initial system. Using the studies of the effect of parameters on case numbers from Table II, we manually test a range of informed parameter choices to replicate features from the real-life data. We start with the simplest combination of compulsory agent parameters (infection threshold, recovery time; the transmission rates and threshold increase factor are set to unity, with no decay in the model). We then vary the optional parameters that cause the greatest perturbation to cases such that fewer parameter selections are required to represent real-life dynamics.

TABLE III. Model parameters used to match to COVID-19 data in England. Agent parameters are the same for every agent in the population.

Network parameters	
Number of agents	2500
Power-law degree distribution exponent	3
Agent parameters	
Infection threshold	100
Recovery time	3
Transmission rate	1
Infectious matter decay constant (infected agents)	6
Threshold factor (immunity)	1.6
Immunity decay constant	35
Initial conditions	
Initial percentage of agents with infectious matter	5
Percentage of threshold initially injected into given agents	0.01

Once results from a given set of parameters match well with the data, we perform a grid search on each parameter to choose a value which minimizes the root-mean-squared error between the simulation and real-life data to justify the choice of parameters (Table III).

Due to the scale-free nature of the network, we simulate 2500 agents as a balance between a large numbers of cases (and thus smaller errors) and excessive computational time. We choose a large infection threshold to reduce the computational rounding errors when summing infection amounts. We averaged 100 runs of the simulation, to account for bias in which nodes are initially chosen to be infected, as well as errors from a finite-size, scale-free power-law network generated stochastically [28].

### C. Results and discussion

#### 1. New cases over time

Figure 2 shows that new cases over time from the simulation match well with the England COVID-19 data [31], with a root-mean-squared error of 0.014%, a remarkable result given all agents in the model have the same parameters. The secondary and tertiary peaks are captured well in the simulation, highlighting how the model has memory of previous interactions and immunity, in contrast to existing epidemiological models which peak only once.

The initial peak is wider for the England data than in the simulation, as the effects of coming out of restrictions and thus a weaker connected network may be delayed and hence the wider peak. The fourth and fifth peaks are less well captured in the simulation, which may be due to the simulation having a fixed population and so may not capture the new cases over time that arise due to a nonzero birth rate, as well as no additional infectious matter arising from travel between countries.

We also note that the fraction of new cases in the population for the simulation is approximately 100 times larger than in England. This suggests that the spread of infection in the model is much greater compared to real-life transmission,

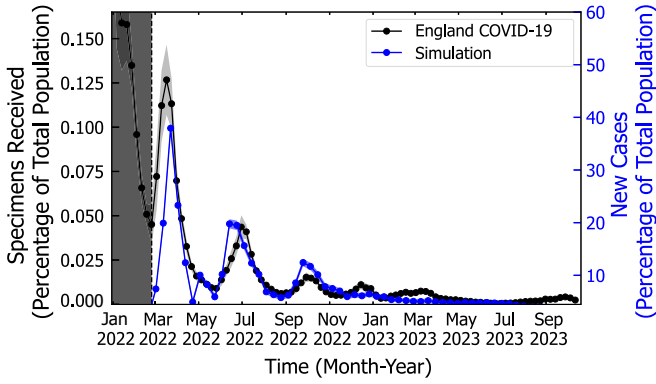


FIG. 2. Comparison of COVID-19 cases in England with new cases from simulations as a percentage of the population. The population of England is assumed to be constant at 56 490 048 [33]. The simulation has 2500 agents, with parameters detailed in Table III. The y axis has been shifted and the x axis scaled to match the England case data. The black curve is the England COVID-19 data [31] and the light-gray shading is the standard deviation from a seven-day average of cases. The dark-gray shading highlights the period where government restrictions were active in England, ending on February 24, 2022 [32]. The blue curve shows the simulation results and blue shading shows the standard deviation from 100 runs.

making measures, such as the number of times agents are re-infected, unrepresentative of real-life dynamics, even though the model captures general features observed in real-life transmission when scaled.

2. Parameters

We scale the simulation time steps by 10.33 to align peaks to the real-life data because time in the simulation is arbitrary. Since agent parameters are homogeneous and independent of the specific population structure of England (e.g., young or elderly, and individuals with different health conditions, which differ only by their degree and amount of initial infectious matter), the model parameters can be regarded as averages for the entire population, as in Table IV. This can help inform interventions (e.g., consider vaccinating individuals after 362 days when their natural immunity has decreased).

Biological studies of COVID-19 report recovery times between 5 and 30 days [34–38], with loss of immunity reported as more uncertain, with protection against reinfection decreasing by  $1/e$  in 275 days if we assume exponential decay [39]. Our parameters fall close to this range, suggesting that the model could be tuned and used in reverse as well by using biological parameters to predict the resulting case numbers.

TABLE IV. Time parameters in the COVID-19 simulation after being scaled to match England’s case data, using one time step equal to 10.33 days.

	Susceptible	Infected
Recovery time		31.00 days
Infectious matter decay constant		62.00 days
Immunity decay constant	361.67 days	361.67 days

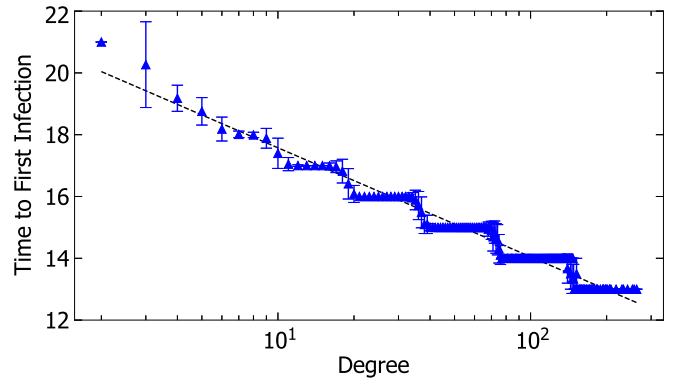


FIG. 3. Semilogarithmic plot of time to first infection against degree. Blue points are the mean and standard deviation from 100 simulation runs using parameters as in Table III. Dashed black line shows a linear fit, with gradient of  $-1.5323 \pm 0.0005$  and y intercept of  $21.104 \pm 0.009$ .

3. Time to first infection

Figure 3 shows how the time to first infection of an agent in the simulation varies with degree. The time to infection decreases with degree, where the next to become infected are those with smaller degrees. Note that there are bands of infection times for given sized groups of degrees, with each time to infection band differing by 1 time step due to the discrete definition of time in the model. The bands become less defined for smaller degrees due to the finite-size power-law network.

Applying a linear regression fit on the semilogarithmic plot, we obtain that for a node with a given degree  $k$ , the time to first infection is approximately  $e^{3.0982k-0.0995}$ , allowing us to predict when agents with a given number of connections will be infected once scaling the result by one time step equals 10.33 days. Recall that we can also calculate the time to first peak in new cases using (5) from the SM [26], as discussed in Sec. II C.

High-degree nodes are infected first, which is consistent with our expectations that well-connected individuals may be infected sooner, illustrated further in a visualization of the network [40] in Fig. 4 where they are among the first to become infected, confirming that high-degree nodes (i.e., well-connected individuals) are indeed propagators of infection.

IV. INTERVENTIONS

A. Method

We test interventions on the England COVID-19 model with the parameters from Table III, as they were shown to capture the observed dynamics of transmission. We study the effect on new cases over time after implementing interventions after 16 time steps, to represent policies put into place as a response to the spread of infection. We assume all agents follow the interventions. Since our model has memory of both previous interactions and immunity, we can also study the effect of removing the intervention. All interventions end after 65 time steps, as it is unlikely that policies will be effective indefinitely.

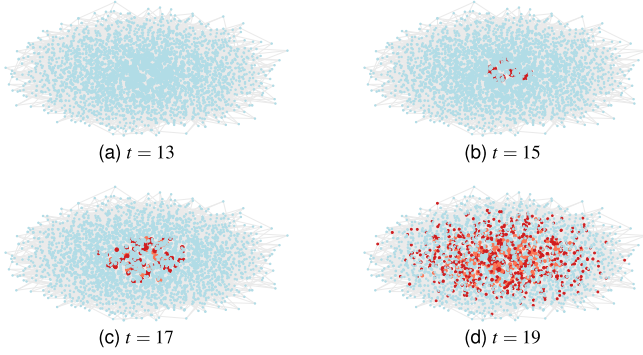


FIG. 4. Snapshots of infection spreading through a network, over time  $t$ , on simulations with COVID-19 parameters as in Table III. Nodes (agents) are represented by circles, which are connected by lines (edges). The size of the node is proportional to the degree of the agent. Blue nodes are susceptible, and dark red nodes have just been infected, fading to lighter shades of red as they progress through the recovery time.

### 1. Quarantine intervention

When agents become infected, we isolate them immediately. In the model, we change their transmission status to inactive and perform transmissions only between active nodes. This is, in effect, temporarily removing infected nodes from the network, representing isolation from their social connections. After the recovery time, the node becomes active and susceptible again.

We can extend this level of quarantine to include isolating the nearest neighbors of an agent for the same length of time, to represent how, by using initiatives such as “test and trace” [41], nations can track who have been in contact with infected agents and instruct them to isolate as well. This is effectively temporarily removing a cluster containing the infected agent and their connections from the network. Both types of isolation are shown in Fig. 5.

### 2. Gathering restrictions

We study the effect of restricting social gatherings by limiting the number of individuals that can meet in a group, e.g., “rule of 6” restrictions that were observed in England [42]. This is implemented by limiting the number of nearest neighbors an agent meets at every time step, ensuring the number of interactions does not exceed the restricted value; otherwise, we try the next-nearest neighbor in the list. We randomize the order of looping through the list to avoid any bias in choosing

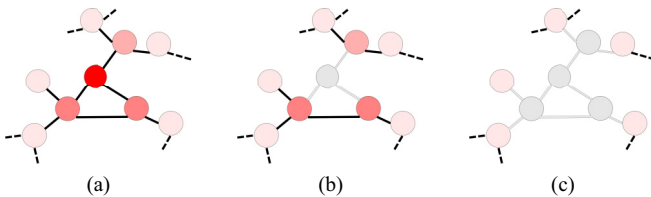


FIG. 5. An extract of a network, where the circles are nodes (agents) and the lines between them are edges (connections). The darker the shade of red, the more infectious matter present in the agent. (a) No intervention, (b) isolate infected, and (c) isolate infected and their nearest neighbors.

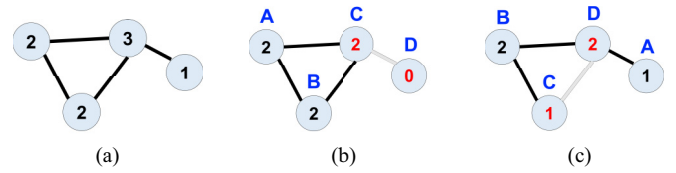


FIG. 6. An extract of a network, where circles are nodes (agents) and connected by gray edges if made inactive by gathering restrictions. Letters are the order in which nodes are visited in the algorithm to implement the restriction. Different orders result in different network configurations. The numbers indicate the degree of the nodes. (a) No intervention; (b) and (c) gathering restriction of 2, where nodes are red if their degree has temporarily changed in the given time step due to the restriction.

which agents meet (Fig. 6). Restrictions cause the network to become more sparsely connected. Clusters of nodes may even become disconnected from the network.

## B. Results and discussion

Figure 7 shows new cases over time for each intervention. The stronger the intervention, the lower the initial peak, with the interventions flattening the curve for new cases. However, as our model has memory of previous interactions and immunity, the stronger the intervention, the higher the secondary peak when the intervention is stopped, suggesting that the intervention has delayed the time to herd immunity. Indeed, the cumulative number of cases for each scenario reach the same value (to within error), highlighting how interventions change only the distribution of the occurrence of new cases. We also note that social gathering restrictions delay the time for new cases to peak, as more interactions are required to transmit the infection around the sparser susceptible network.

## V. MULTISTRAIN

### A. Implementation

The single-strain model can be extended to multiple strains by studying their interplay and competition in a population. We consider two strains  $X$  ( $X = A, B$ ), each with its own parameters (i.e., infection thresholds, recovery times, transmission rates, and decay constants). The strains transmit independently of each other through the network, with agents adding the transmitted infection for each strain separately. However, when infectious matter exceeds the threshold for a given strain, the agent stops receiving for both strains, representing how unlikely it is for an individual to simultaneously become infected with both strains [43]. If the threshold for both strains is exceeded at the same time, although rare [43], we declare the node as infected with both strains (to avoid bias), for the longer recovery time. On recovery, the amount of infectious matter is reset to zero for both strains.

We introduce cross immunity, representing how individuals gain immunity to other strains on recovery [44]. The threshold increase factors are, in matrix form,

$$F = \begin{pmatrix} F_{AA} & F_{AB} \\ F_{BA} & F_{BB} \end{pmatrix}, \quad (1)$$

where  $F_{ij}$  is the infection threshold increase of strain  $j$  after being infected with strain  $i$ . For example, for an agent

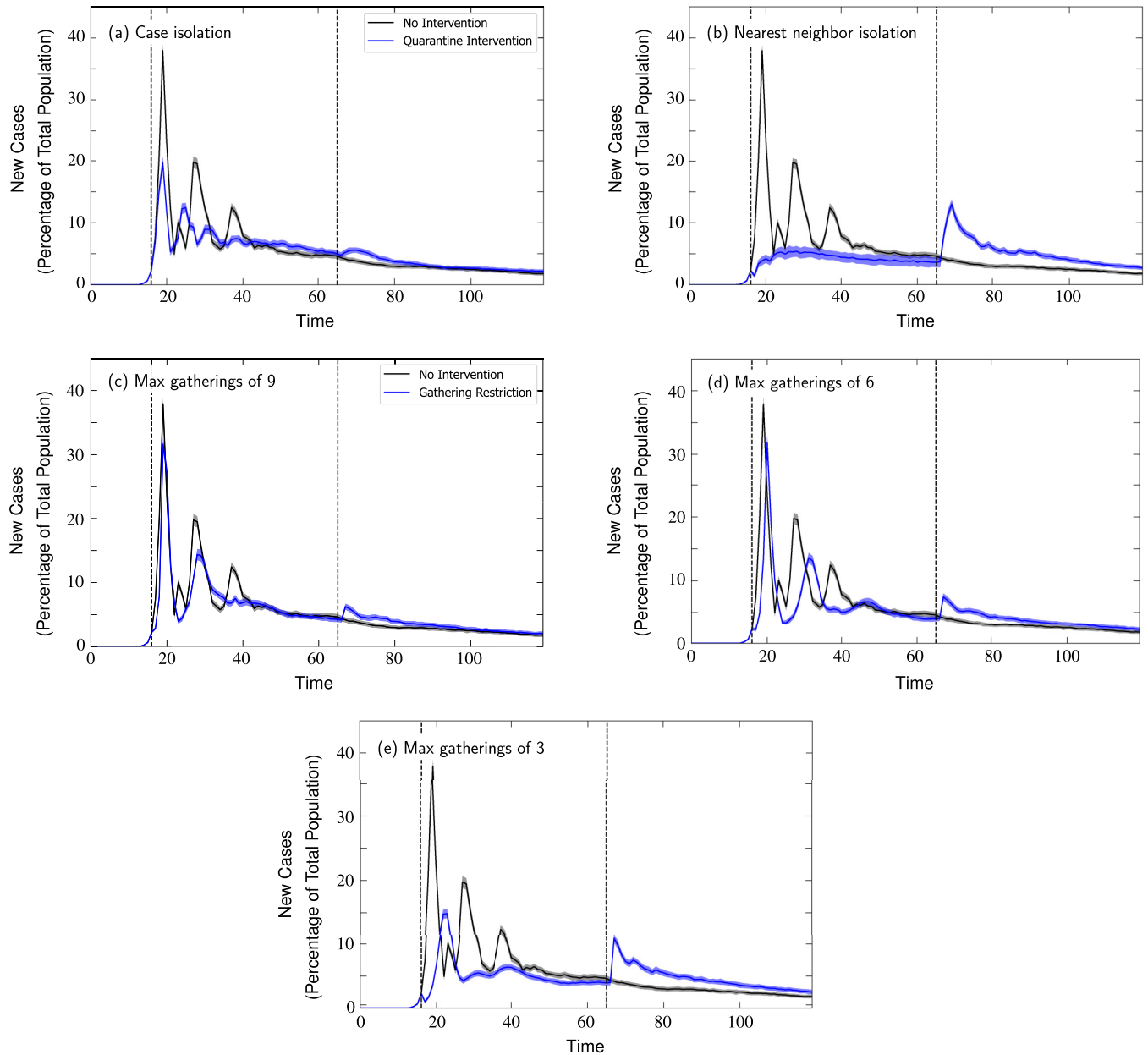


FIG. 7. New cases over time, averaged over 100 simulation runs, with various interventions in place with COVID-19 model parameters (Table III). Black curves indicate no intervention; blue curves indicate interventions starting at time step 16 and ending at time step 65. Shaded regions show standard deviation. (a) Case isolation and (b) case and nearest-neighbor isolation. Gatherings restricted to (c) no larger than 9, (d) no larger 6, and (e) no larger than 3.

recovered from strain A, their strain A threshold increases by a factor  $F_{AA}$  and their strain B threshold by a factor  $F_{AB}$ . There is one epidemiological state of susceptibility, but now two states for infection (with strain A or B), returning to the susceptible state in different ways as their thresholds change differently.

## B. Influenza

### 1. Real-life data set

We compare our multistrain model against the Canada influenza case data [45] since it spreads through close-contact human interaction [46], and there are two strains, with strain

A being more commonly found than strain B [47]. We track positive influenza specimens received as new cases, and do not consider data from 2020 onwards due to the COVID-19 pandemic and government restrictions affecting case numbers.

### 2. Tuning the model

We begin tuning the simulation parameters by keeping parameters for both strains the same so we can use the results from the studies in Sec. II C. The only agent parameter we vary between the strains is the transmission rate, with strain A being more contagious and having a longer recovery time. We choose a symmetric matrix for the threshold increase factor

TABLE V. Model parameters used to match influenza strain-A and strain-B data in Canada. Agent parameters are the same for every agent in the population, and the transmission rate and infectious matter decay constant are the same for both susceptible and infected agents.

Network parameters		
Number of agents	2500	
Power-law degree distribution exponent	3	
Agent parameters	Strain A	Strain B
Infection threshold	100	100
Recovery time	40	20
Transmission rate	1	0.965
Infectious matter decay constant	4	4
Threshold factor (immunity)	$\begin{pmatrix} 5 & 3 \\ 3 & 5 \end{pmatrix}$	
Immunity decay constant	52	52
Initial conditions	Strain A	Strain B
Initial percentage of agents with infectious matter	0.5	0.5
Percentage of threshold initially injected into given agents	1	10

for simplicity. We initially inject more of strain B into the system to test if the model dynamics correctly lead to strain A overtaking to become the dominant strain. We also remove the output factor (which previously scaled with immunity) to introduce periodic peaking in the model and to encapsulate the fast-mutating strain A and strain B subtypes (leading to typical annual infection rounds) [48].

After visually comparing the shape of simulation results to real-life data, followed by a refinement with a grid search and by minimizing the root-mean-squared error, the resulting model parameters are listed in Table V. We scale the simulation time steps by 10.60 to align to the real-life data. Note that the recovery time is much larger than the 3–7 days expected in real life [49]. In this case, the infectious matter decay constant is much less than the recovery time. Thus, the agent will have infectious matter close to zero, analogous to “recovering,” but will not receive infectious matter due to still being in the “infected” state. This allows us to reinterpret the recovery time to include the time the agent can no longer get reinfected and become susceptible again.

### 3. Results and discussion

Figure 8 compares the number of cases over time observed in Canada with simulations, which well capture the alteration between strains, with a root-mean-squared error of 0.002% and 0.0012% for strain A and B, respectively. We did not take weekly averages of cases as no dip in the received specimens was seen towards the end of the week. There is no error shown in the simulation results, as the extract of simulation results matching the real-life data set changes each simulation run, highlighting the sensitivity of the multistrain model to which nodes are randomly initially injected with infectious matter.

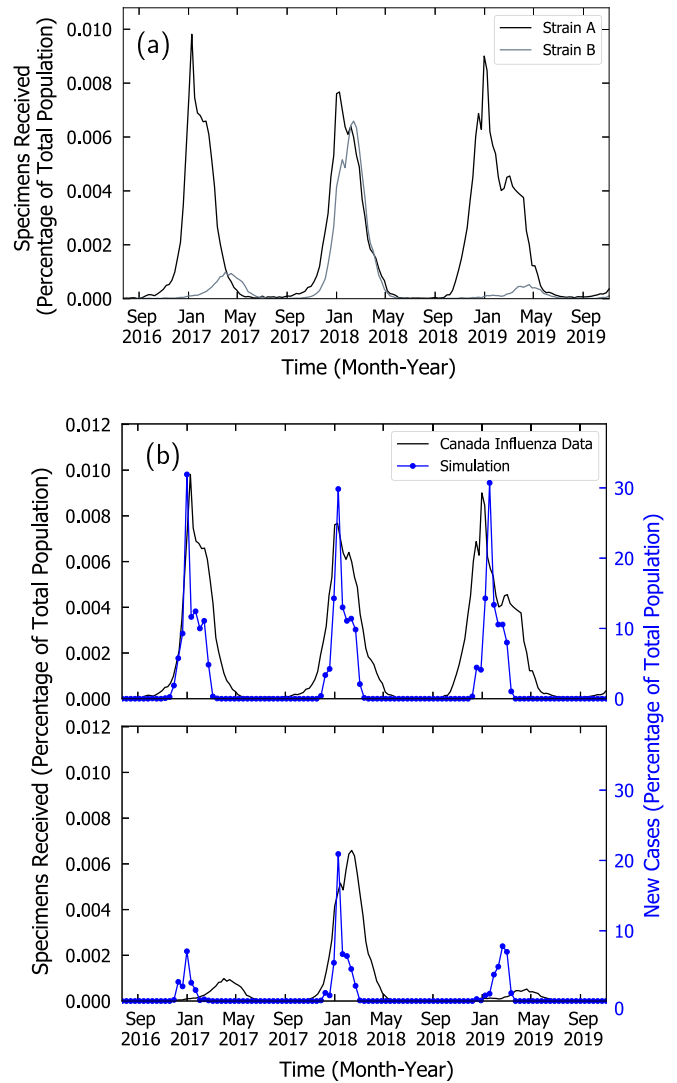


FIG. 8. (a) Canada influenza data [45], for strain A (black) and strain B (gray). (b) Blue curve is simulation results using the parameters in Table V, against Canada’s strain A case data in the black curve in the top graph, and strain B in the gray curve in the bottom graph. There is no error since this is an extract of one run lined up to match the real-life data.

However, the width of the peaks in the simulation is narrower than observed in Canada. This suggests that the simulation network is more strongly connected than in real life, so the infection spreads faster. This is consistent with Sec. IV, where we saw sparser networks due to gathering restrictions widening peaks in new cases. Furthermore, the population by region in Canada varies drastically [50] and has a much lower population density compared to England that previously matched well ( $\sim 4$  people per square kilometer [51] vs  $\sim 400$  people per square kilometer [52]), so a different power-law degree distribution exponent may be required, or a different network may be more suitable to capture the scale of transmission, for example, a random-partition graph.

Second, there is an offset observed in the real-life data, with strain B peaking after strain A, though in the model they

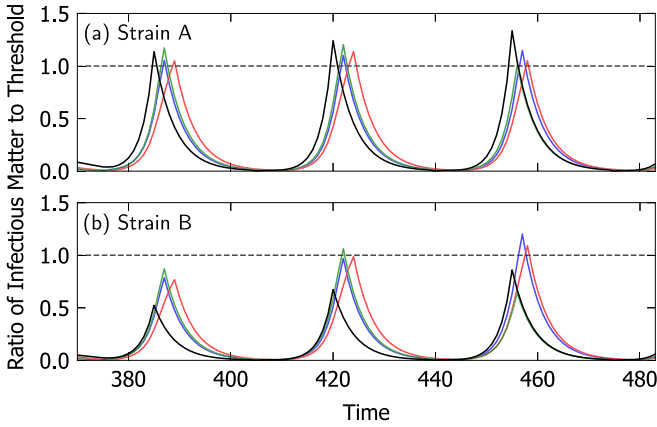


FIG. 9. Ratio of infectious matter to threshold over time for a cluster containing a randomly selected node (black curve) and its nearest neighbors (red, blue, and green curves). A node is infected when the value exceeds unity.

peak at the same time. We suspect this is due to both of the strains following the same dynamics. We saw in Sec. III C that the first to become infected and thus the main propagators of infection are high-degree nodes. Since both strains spread in the same way and reach the high-degree nodes in the same way, the two strains that are peaking may become synchronized. Furthermore, since an agent stops receiving infectious matter for both strains when infected with one, and the infectious matter is reset to zero for both on recovery, unwanted coupling between the two strains may have been introduced. To alleviate this, the multistrain dynamics could be adjusted such that on recovery, a given fraction of the infectious matter from the other strain remains.

We zoom into a randomly selected agent, plotting the ratio of infectious matter to threshold of that agent (to normalize it to account for the changing threshold due to immunity) over time, alongside its nearest neighbors, in Fig. 9. The rise and fall for both strains look similar since the dynamics of transmission are the same, though with the slope of strain A appearing steeper, illustrating the faster accretion of infectious matter due to the higher transmission rate. However, we note that the randomly selected node always becomes infected first for strain A in relation to its nearest neighbors, illustrating that it is a driver of infection within this cluster and such drivers of infection exist throughout the network.

We average the ratio of infectious matter to threshold over all agents in the system for each time step, as shown in Fig. 10. We note that this is the quantity  $\bar{I}(t)$  in (3) of the SM [26] (adjusted for our system size). This can be reinterpreted as the probability that a randomly selected node is infected at a given time. Nodes, on average, are initially more likely to be infected with strain B due to more of this strain in the system initially, but strain A quickly dominates, with the probability of being infected with strain A always higher than with strain B, consistent with strain A being more commonly found in real life [47]. We again notice the synchronicity in peaking for both strains, suggesting that injecting strain A into the system after strain B has already peaked may help introduce the offset observed in real life.

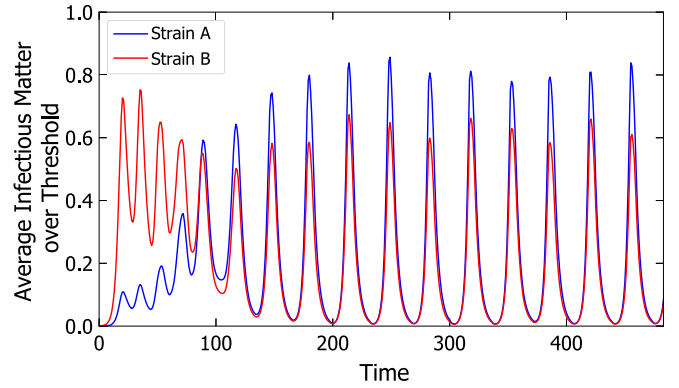


FIG. 10. Amount of infectious matter over threshold, averaged over all the agents in the population, over time. There is initially more of strain B in the system, but strain A quickly dominates. There is no error since it corresponds to a single simulation run. Strain A is indicated by the blue curve; strain B by the red curve.

## VI. CONCLUSION AND FURTHER WORK

We have created a model of disease transmission on a network with integrate-and-fire nodes, giving memory of previous interactions and infections. We have demonstrated its feasibility in terms of accurately modeling disease transmission of COVID-19 in England and multiple strains of influenza in Canada, capturing the secondary peaks in new cases compared to existing models, and allowing interventions to be tested to inform policymaking.

Agents in a power-law network sum infectious matter from their nearest neighbors (social connections) at every time step until they exceed their infection threshold, at which point they become infected for as long as the recovery time. Immunity is modeled by increasing their infection threshold on recovery. Studying the dynamics of the model with a simulation reveals the effect of each parameter on case numbers, with there being no new cases when the infectious matter decay constant is less than  $1/\ln 2$ . The time to first peak in new cases for any system size is the same as the analytical expression for time to first infection for two agents. Visualizations further reveal that agents with a higher number of connections are the main drivers of infection.

We found the single-strain version of the model to match well with the dynamics of real-life disease transmission when compared against COVID-19 case numbers in England, giving a root-mean-squared error of 0.014%. Extending the model to multiple strains by introducing cross immunity, we show the model can replicate features of the spread of influenza in Canada to a root-mean-squared error of 0.002% and 0.0012% for strain A and B, respectively. These are remarkable results, given the model has homogeneous agent parameters, with distributions of agent parameters (e.g., recovery time) not required to match to the specific population and demographic structure of the country. Further investigation is required into removing the synchronicity seen in the peaking of multiple strains (which is not observed in nature) by performing a full study of the effect of each model parameter in the multistrain version, as conducted with the single-strain version. Finally, we find quarantining and

social-gathering restrictions to lower peaks in new cases in the model. Importantly, we find that the stricter the intervention, the larger the secondary wave of peaks when the intervention is removed due to the model having memory.

Further work includes adding an intermediate stage to the susceptible-infected-susceptible integrate-and-fire model, where infected agents can enter a hospitalization state with a given probability. The hospitalization state can have different parameters (e.g., longer recovery time) and can mean that we can study the impact on hospital capacity. Furthermore, the model can be extended for variable populations by introducing birth rates (by adding more nodes through preferential attachment to the existing network) and death rates (by having a probability for each state of removing the node from the network). The model can also be extended to an open system, where infectious matter is injected into the system not just

initially, but also at later time steps, to simulate the effects of travel between countries.

We can also study the impact of vaccinations by randomly selecting nodes to increase their threshold, instead of just modeling natural immunity. Different vaccination strategies can be investigated, e.g., randomly vaccinating some percentage of the population at each time step, selecting nodes with a given degree or with less than a given number of previous infections.

Our existing multistrain version of the model can be extended to any number of “strains” to study how different infections interact in the same population. For example, an agent infected with tuberculosis may increase their probability of being infected with COVID-19 [53], implemented by lowering their threshold. This will give memory of previous health conditions in the model.

- 
- [1] D. McAdams, Nash SIR: An economic-epidemiological model of strategic behavior during a viral epidemic, *Covid Econ.* **16**, 115 (2020).
- [2] I. Cooper, A. Mondal, and C. G. Antonopoulos, A SIR model assumption for the spread of COVID-19 in different communities, *Chaos Soliton Fract.* **139**, 110057 (2020).
- [3] L. A. Meyers, M. E. J. Newman, M. Martin, and S. Schrag, Applying network theory to epidemics: Control measures for *mycoplasma pneumoniae* outbreaks, *Emerg. Infect. Dis.* **9**, 204 (2003).
- [4] M. E. J. Newman, Spread of epidemic disease on networks, *Phys. Rev. E* **66**, 016128 (2002).
- [5] K. Hamilton, P. Date, B. Kay, and C. D. Schuman, Modeling epidemic spread with spikebased models, in *ICONS 2020: International Conference on Neuromorphic Systems 2020* (Association for Computing Machinery (ACM), New York, 2020), pp. 1–5.
- [6] D. McAdams, The blossoming of economic epidemiology, *Annu. Rev. Econom.* **13**, 539 (2021).
- [7] M. Kamo and A. Sasaki, The effect of cross-immunity and seasonal forcing in a multi-strain epidemic model, *Physica D* **165**, 228 (2002).
- [8] F. Iannelli, A. Koher, D. Brockmann, P. Hövel, and I. M. Sokolov, Effective distances from epidemic spreading on complex networks, *Phys. Rev. E* **95**, 012313 (2017).
- [9] C. R. Lucatero, Analysis of epidemic models in complex networks and node isolation strategic proposal for reducing virus propagation, *Axioms* **13**, 79 (2024).
- [10] T. Granger, T. M. Michelitsch, M. Bestehorn, A. P. Riascos, and B. A. Collett, Stochastic compartment model with mortality and its application to epidemic spreading with complex networks, *Entropy* **26**, 362 (2024).
- [11] M. Saeedian, M. Khalighi, N. Azimi-Tafreshi, G. R. Jafari, and M. Ausloos, Memory effects on epidemic evolution: The susceptible-infected-recovered epidemic model, *Phys. Rev. E* **95**, 022409 (2017).
- [12] M. Tizzani, S. Lenti, E. Ubaldi, A. Vezzani, C. Castellano, and R. Burioni, Epidemic spreading and aging in temporal networks with memory, *Phys. Rev. E* **98**, 062315 (2018).
- [13] X. R. Hoffman and M. Boguña, Memory-induced complex contagion in epidemic spreading, *New J. Phys.* **21**, 033034 (2019).
- [14] M. Bestehorn, T. M. Michelitsch, B. A. Collet, A. P. Riascos, A. F. Nowakowski, Simple model of epidemic dynamics with memory effects, *Phys. Rev. E* **105**, 024205 (2022).
- [15] L. Basnarkov, I. Tomovski, T. Sandev, and L. Kocarev, Non-Markovian SIR epidemic spreading model COVID-19, *Chaos, Solitons Fractals* **160**, 112286 (2022).
- [16] M. Feng, L. Tian, Y.-C. Lai, and C. Zhou, Validity of Markovian modeling for transient memory-dependent epidemic dynamics, *Commun. Phys.* **7**, 86 (2024).
- [17] C. Li, J. Wang, J. Xu, and Y. Rong, The global dynamics of a SIR model considering competitions among multiple strains in patchy environments, *Math. Biosci. Eng.* **19**, 4690 (2022).
- [18] M. T. Sofonea, B. Reyné, B. Elie, R. Djidjou-Demassee, C. Selinger, Y. Michalakis, and S. Alizon, Memory is key in capturing COVID-19 epidemiological dynamics, *Epidemics* **35**, 100459 (2021).
- [19] H. Heesterbeek, R. M. Anderson, V. Andreasen, S. Bansal, D. De Angelis, C. Dye, K. T. D. Eames, W. J. Edmunds, S. D. W. Frost, S. Funk, T. D. Hollingsworth, T. House, V. Isham, P. Klepac, J. Lessler, J. O. Lloyd-Smith, C. J. E. Metcalf, D. Mollison, L. Pellis, J. R. C. Pulliam, M. G. Roberts, and C. Viboud (Isaac Newton Institute IDD Collaboration), Modeling infectious disease dynamics in the complex landscape of global health, *Science* **347**, aaa4339-1 (2015).
- [20] N. C. Grassly and C. Fraser, Mathematical models of infectious disease transmission, *Nat. Rev. Microbiol.* **6**, 477 (2008).
- [21] R. Pastor-Satorras, C. Castellano, P. Van Mieghem, and A. Vespignani, Epidemic processes in complex networks, *Rev. Mod. Phys.* **87**, 925 (2015).
- [22] J. Bedson, L. A. Skrip, D. Pediti, S. Abramowitz, S. Carter, M. F. Jalloh, S. Funk, N. Gobat, T. Giles-Vernick, G. Chowell, J. R. de Almeida, R. Elessawi, S. V. Scarpino, R. A. Hammond, S. Briand, J. M. Epstein, L. Hébert-Dufresne, and B. M. Althouse, A review and agenda for integrated disease models including social and behavioral factors, *Nat. Hum. Behav.* **5**, 834 (2021).
- [23] L. M. Lopicque, Recherches quantitatives sur l’excitation électrique des nerfs traitée comme une polarisation, *J. Physiol.*

- Pathol. Gen. **9**, 620 (1907); Translation: N. Brunel and M. C. W. van Rossum, Quantitative investigations of electrical nerve excitation treated as polarization, *Biol. Cybern.* **97**, 341 (2007).
- [24] W. Gerstner, W. M. Kistler, R. Naud, and L. Paninski, *Neuronal Dynamics: From Single Neurons to Networks and Models of Cognition* (Cambridge University Press, Cambridge, 2014).
- [25] I. N. Lympelopoulous and G. D. Ioannou, Online social contagion modeling through the dynamics of integrate-and-fire neurons, *Inf. Sci.* **320**, 26 (2015).
- [26] See Supplemental Material at <http://link.aps.org/supplemental/10.1103/PhysRevE.110.014305> for an derivation of solutions to the two-agent problem, the algorithm used for the simulations reported here, and showing how varying the parameters changes disease transmission in our model.
- [27] R. Albert and A.-L. Barabási, Statistical mechanics of complex networks, *Rev. Mod. Phys.* **74**, 47 (2002).
- [28] A.-L. Barabási, *Network Science* (Cambridge University Press, Cambridge 2017).
- [29] <https://www.python.org>
- [30] R. Karia, I. Gupta, H. Khandait, A. Yadav, and A. Yadav, COVID-19 and its modes of transmission, *SN Compr. Clin. Med.* **2**, 1798 (2020).
- [31] UK Coronavirus dashboard (2018), <https://coronavirus.data.gov.uk>.
- [32] Prime minister sets out plan for living with COVID (2022), <https://www.gov.uk/government/news/prime-minister-sets-out-plan-for-living-with-covid>.
- [33] M. Roskams, Population and household estimates, England and Wales: Census 2021, unrounded data (2022), <https://www.ons.gov.uk/peoplepopulationandcommunity/populationandmigration/populationestimates/bulletins/populationandhouseholdestimatesenglandandwales/census2021unroundeddata>.
- [34] O. S. Ibitoye, Y. A. Olasunkanmi, T. A. Olowolafe, A. T. Olabode, M. M. Salawu, and R. F. Afolabi, Predictors and time to recovery from COVID-19 among patients attended at the treatment centers in Ekiti state, South West Nigeria, *Pan. Afr. Med. J.* **42**, 18 (2022).
- [35] A. W. Kaso, H. E. Hareru, T. Kaso, and G. Agero, Time to recovery from Covid-19 and its associated factors among patients hospitalized to the treatment center in South Central Ethiopia, *Environ. Chall.* **6**, 100428 (2022).
- [36] S. Tsegaye, F. Bekele, Y. Lulu, G. R. Debele, T. Bekana, L. D. Tolesa, and K. Bidira, Time to recovery and its predictors among COVID-19 positive patients admitted to treatment centers and Southwestern Ethiopian hospitals. A multicenter retrospective cohort study, *Ann. Med. Surg.* **84**, 104917 (2022).
- [37] G. Churiso, K. Diriba, H. Girma, and S. Tafere, Clinical features and time to recovery of admitted COVID-19 cases at Dilla University referral hospital treatment center, South Ethiopia, *Infect. Drug Resist.* **15**, 795 (2022).
- [38] B. Liu, D. Jayasundara, V. Pye, T. Dobbins, G. J. Dore, G. Matthews, J. Kaldor, and P. Spokes, Whole of population-based cohort study of recovery time from COVID-19 in New South Wales Australia, *Lancet Reg. Health West. Pac.* **12**, 100193 (2021).
- [39] C. Stein, H. Nassereldine, R. J. D. Sorensen, J. O. Amlag, C. Bisignano, S. Byrne, E. Castro, K. Coberly, J. K. Collins, J. Dalos, F. Daoud, A. Deen, E. Gakidou, J. R. Giles, E. N. Hulland, B. M. Huntley, K. E. Kinzel, R. Lozano, A. H. Mokdad, T. Pham *et al.*, Past SARS-CoV-2 infection protection against re-infection: A systematic review and meta-analysis, *Lancet* **401**, 833 (2023).
- [40] A. A. Hagberg, D. A. Schult, and P. J. Swart, Exploring network structure, dynamics, and function using NetworkX, in *Proceedings of the 7th Python in Science Conference (SciPy2008)*, edited by G. Varoquaux, T. Vaught, and J. Millman (Pasadena, CA, 2008), pp. 11–15.
- [41] Test and trace: What to do if you are contacted (2020), <https://www.gov.uk/guidance/nhs-test-and-trace-how-it-works>.
- [42] Rule of six comes into effect to tackle Coronavirus (2020), <https://www.gov.uk/government/news/rule-of-six-comes-into-effect-to-tackle-coronavirus>.
- [43] A. S. Leonard, M. T. McClain, G. J. D. Smith, D. E. Wentworth, R. A. Halpin, X. Lin, A. Ransier, T. B. Stockwell, S. R. Das, A. S. Gilbert, R. Lambkin-Williams, G. S. Ginsburg, C. W. Woods, K. Koelle, and C. J. R. Illingworth, The effective rate of influenza reassortment is limited during human infection, *PLoS Pathog.* **13**, e1006203 (2017).
- [44] V. Andreasen and S. Sasaki, Shaping the phylogenetic tree of Influenza by cross-immunity, *Theor. Popul. Biol.* **70**, 164 (2006).
- [45] World Health Organization, FluNet, <https://www.who.int/tools/flu-net>.
- [46] Centers for Disease Control and Prevention, How flu spreads (2022), <https://www.cdc.gov/flu/about/disease/spread.htm>.
- [47] Centers for Disease Control and Prevention, Types of Influenza viruses (2023), <https://www.cdc.gov/flu/about/viruses/types.htm>.
- [48] E. Nobusawa and K. Sato, Comparison of the mutation rates of human Influenza A and B viruses, *J. Virol.* **80**, 3675 (2006).
- [49] Public Health Agency of Canada, Flu (Influenza): For health professionals (2023), <https://www.canada.ca/en/public-health/services/diseases/flu-influenza/health-professionals.htm>.
- [50] Government of Canada, Statistics Canada, Population and demography (2008), [https://www150.statcan.gc.ca/n1/pub/11-402-x/2008/3867/ceb3867\\_000-eng.htm](https://www150.statcan.gc.ca/n1/pub/11-402-x/2008/3867/ceb3867_000-eng.htm).
- [51] World Bank Open Data, Population density (people per sq. km of land area)-Canada, <https://data.worldbank.org/indicator/EN.POP.DNST?locations=CA>.
- [52] Office for National Statistics, Population density (2021), <https://www.ons.gov.uk/datasets/TS006/editions/2021/versions/4>.
- [53] D. Visca, C. W. M. Ong, S. Tiberi, R. Centis, L. D'Ambrosio, B. Chen, J. Mueller, P. Mueller, R. Duarte, M. Dalcolmo, G. Sotgiu, G. B. Migliori, and D. Golettin, Tuberculosis and COVID-19 interaction: A review of biological, clinical and public health effects, *Pulmonology* **27**, 151 (2021).